Incommensurate modulation and the crystal structure of ganophyllite

DAVID CHRISTOPHER NOE* AND DAVID R. VEBLEN

Department of Earth and Planetary Sciences, The Johns Hopkins University, Baltimore, Maryland 21218, U.S.A.

ABSTRACT

Incommensurate modulation in ganophyllite crystals was investigated with selected-area electron diffraction (SAED), high-resolution transmission electron microscopy (HRTEM), analytical electron microscopy (AEM), and single-crystal X-ray diffraction (XRD) techniques. The XRD data were used to perform a new subcell ($a = 5.550$ Å, $b = 13.539$ Å, $c = 25.134$ Å, $\beta = 93.928°$) refinement of the structure with a higher precision than previous refinements ($R = 0.041$). Although supercell reflections were too weak for collection with the diffractometer, the supercell was modeled by comparing experimental SAED patterns and HRTEM images to their simulated counterparts. These simulations indicate that incommensurate modulation arises from offsets in the location of inverted tetrahedra between adjacent [100] strips. The true supercell of incommensurate crystals involves a tripling of the subcell **a** axis and at least a twelvefold increase in the **b** axis; previously identified supercell reflections are actually aggregates of extremely closely spaced reflections in incommensurate crystals. Unlike commensurate crystals, the subcell **c** axis of incommensurate ganophyllite is not doubled. AEM data suggest that the occurrence of commensurate or incommensurate forms is not compositionally dependent.

INTRODUCTION

Ganophyllite is a manganese-bearing, modulated layer silicate. As with other minerals in this group (e.g., stilpnomelane, bannisterite, etc.), modulation arises due to a mismatch between relatively large, Mn-rich octahedral sheets and relatively small, Si-rich tetrahedral sheets. Eggleton and Guggenheim (1986) approximated the chemical formula of ganophyllite as $(K,Na,Ca)_6(Mg,Fe,Mn)_{24}[Si_{32.5}Al_{7.5}]O_{96}(OH)_{16}\cdot21H_2O$, $Z = 8$. The Na end-member of ganophyllite is known as eggletonite (Peacor et al. 1984).

Ganophyllite was first described by Hamberg (1890), but Smith and Frondel (1968) determined that some samples identified as ganophyllite actually contained the previously undescribed mineral bannisterite. They also noted weak superlattice reflections that extended a body-centered subcell. Based upon X-ray precession photographs, they suggested a supercell ($a = 16.60$ Å, $b = 27.04$ Å, $c = 50.34$ Å, $\beta = 94.3°$) with Aa or $A2/a$ symmetry that involved tripling of the subcell along **a** and doubling along both **b** and **c**. Smith and Frondel (1968) also noted that samples had a micaceous cleavage parallel to (001) with secondary cleavages along (100) and (010), and that this was consistent with a modified layer structure or a combination of sheet and chain structures.

Jefferson (1978) reported the occurrence of both monoclinic and triclinic varieties of ganophyllite based upon X-ray pre-

cession photographs. Cell constants for the monoclinic supercell were consistent with those of Smith and Frondel (1968); cell constants for the triclinic form indicated a tripling of the subcell along **a**, quadrupling along **b**, and no increase along **c**. Jefferson (1978) used "structural column" models to examine the supercell. In this technique, columns parallel to [100] were aligned with different relative displacements along **a**. Models for the triclinic and monoclinic forms were proposed, based upon relative **a**/6 translations of the columns.

Kato (1980) performed a single-crystal structure refinement of the subcell. This refinement ($R = 0.078$) demonstrated that the lateral misfit between a Mn octahedral sheet and Si tetrahedra was accommodated by a modified layer structure, in which the tetrahedral sheet was rifted into triple chains along [100]. It also demonstrated that the octahedral sheet has a sine-wave like morphology along [010]. The interlayer cation was placed between rifts in adjacent sheets, along with associated water molecules. Modulation was attributed to the ordering of interlayer cations and water molecules in the interlayer and site preferences for Al in the tetrahedral sheet.

Eggleton and Guggenheim (1986) used the data of Kato (1980) to re-refine the subcell structure. This refinement ($R = 0.097$) identified the presence of inverted tetrahedra near the rifted area, which extend into the interlayer. These tetrahedra (Si4 and Si5) share apical O atoms with inverted tetrahedra from the adjacent sheet. The inverted tetrahedra are similar in structural function to those of other manganese phyllosilicates, notably stilpnomelane and bannisterite. The occupancy of inverted tetrahedra was found to be approximately 1/3, whereas the occupancy of adjacent tetrahedra (T3) at the edge of the

FIGURE 1. The crystal structure of ganophyllite. Data from the new subcell refinement.

commensurate

incommensurate

FIGURE 2. Commensurate and incommensurate [$hk0$] SAED patterns of ganophyllite.

triple chains was found to be approximately 2/3. These occupancies were identified as producing the threefold modulation along [100]. The doubling of **b** and **c** was attributed to different patterns of occupancies in the Si3, Si4, and Si5 positions in adjacent [100] strips (Fig. 1). Eggleton and Guggenheim (1986) also proposed both monoclinic and triclinic forms as a function of this displacement.

Modulation in ganophyllite results in tripling of the **a** axis and the introduction of weak superlattice reflections in diffraction patterns. These superlattice reflections, together with the corresponding sublattice reflections, are visible in rows along **a***. A careful examination of SAED patterns indicates that superlattice reflections for many crystals of ganophyllite are rotated out of the reciprocal lattice rows, indicating that the modulation is not commensurate with the crystallographic axes of the subcell (Fig. 2). The amount of incommensurate rotation was found to vary from zero (apparently commensurate) to approximately three degrees. This incommensurate modulation is not accounted for by the model of Eggleton and Guggenheim (1986).

To determine the structural nature of such incommensurate modulation, crystals of ganophyllite were examined by SAED, HRTEM, AEM, and XRD. Single-crystal X-ray intensity data
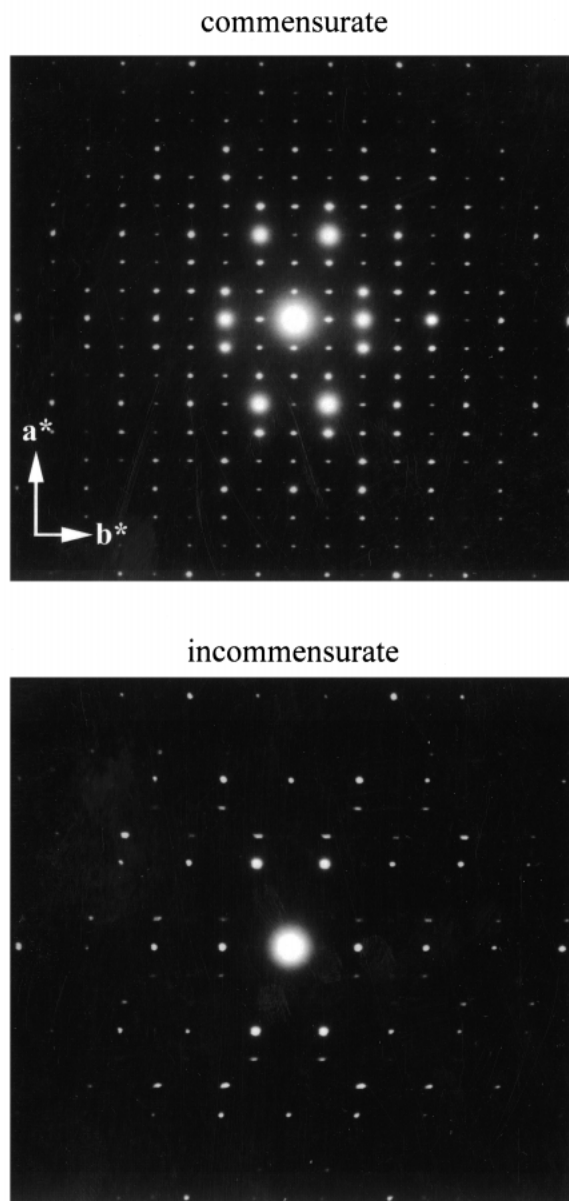
were used to perform a new refinement of the subcell to better characterize the crystal structure. HRTEM lattice images from crystals with different degrees of incommensurate rotation were compared to the corresponding SAED patterns. Because the intensity of supercell diffraction spots could not be measured with the available XRD equipment, experimentally derived SAED patterns and HRTEM images were compared to their simulated counterparts to qualitatively determine the nature of "incommensurate" modulation. Chemical compositions were determined by X-ray emission analytical electron microscopy (AEM) to determine if there was a compositional basis for "incommensurate" modulation.

Considerable work has been published on the structures of

TABLE 1. Crystal data and results of the subcell structure refinement

a (Å)	5.550(2)	Reflections	$\pm h \pm k + l$, for $h + k + l = 2n$
b (Å)	13.539(2)	Scan time (s)	≤ 300
c (Å)	25.134(6)	Scan type	$\omega/2\theta$
β (°)	93.928(5)	Number of data	5829
Symmetry	$I2/a$	Unique data	2888
Crystal dimensions (μm^3)	$120 \times 120 \times 120$	Reflections $I > 3\sigma$	2389
Radiation	Mo$K\alpha$	R	0.041
θ Range (°)	0–45	R_W	0.045

Note: Number in parentheses represents one esd of least significant digit.

modulated minerals with layered and pseudo-layered arrangements, including Heinrich et al. (1994) and Eggleton and Guggenheim (1994a) on the structure of bementite, Eggleton and Guggenheim (1994b) and Guggenheim and Eggleton (1994) on the structure of parsettensite, Ferrow and Hovmøller (1993) and Heaney et al. (1992) on the structure of bannisterite, and Post and Veblen (1990) on the structure of birnessite. The EMU volume on modulated structures is a useful volume on modulated structures in general (Merlino 1997).

EXPERIMENTAL DETAILS

Sample

Crystals from Franklin Furnace, New Jersey, were obtained from private sources and from the U.S. National Museum of Natural History (NMNH 164001); crystals from Pajsberg, Sweden were obtained from the Smithsonian (NMNH B17240). Examination with a polarizing light microscope confirmed that the samples were well crystallized and free of visible inclusions. The crystals were optically biaxial, confirming that their symmetry was orthorhombic or lower. Precession photographs confirmed that the crystals diffracted well and were apparently untwinned.

The crystal selected for data collection was from Franklin Furnace (private collection). Precession photographs confirmed that the subcell symmetry could best be described using the non-standard space group $I2/a$, consistent with Smith and Frondel (1968). SAED patterns, in which supercell spots are much more intense than diffraction patterns formed with X-rays, also confirmed that the supercell symmetry of apparently commensurate ganophyllite is consistent with $A2/a$. The supercell symmetry of the "incommensurate" ganophyllite used in this study is triclinic.

Data collection and structure refinement

An Enraf-Nonius CAD4 diffractometer with graphite-monochromatized Mo radiation (located at the U.S. NMNH) was used for X-ray intensity data collection at 292 K. It was originally intended to collect data for a supercell refinement of the structure; however, it was found that the supercell reflections were too weak for this purpose. It was then decided to collect data for a subcell refinement. Data collection parameters are summarized in Table 1. Unit-cell parameters were obtained from refinement of the setting angles of 25 automatically centered reflections. Initial data reduction was performed using the program MOLEN. Data were reduced and corrected for Lorentz and polarization effects, and a linear correction was applied for intensity decay. Specimen absorption was corrected using psi scans, and equivalent reflections were averaged.

Least-squares calculations were performed in the XTAL3.2 set of programs (Hall et al. 1992). Full-matrix least-squares refinement was performed using data with $I > 3\sigma_I$. The structure was modeled in space group $I2/a$, with initial positional and displacement parameters for the primary (those with high occupancy) positions obtained from Eggleton and Guggenheim (1986). Initial stages of the refinement were conducted with isotropic displacement parameters and fixed occupancies. As the refinement converged, these restrictions were gradually relaxed, and most positions were refined with anisotropic displacement parameters and unconstrained occupancy (Table 2). Table 3[1] contains anisotropic displacement paraments. Positions in the interlayer region were identified from difference and direct Fourier maps and added to the structure. Early in the refinement, it became apparent from the Fourier maps that several of the positions were split. Many of these sites are similar to the split sites reported by Eggleton and Guggenheim (1986); however, some previously unidentified split positions were noted. Once identified, split positions were added to the model.

Due to the lower occupancy and somewhat disordered nature of sites in the interlayer region, positions in this area were difficult to refine. Although clearly visible as discrete peaks of electron density in Fourier maps, several positions in the interlayer had to be refined with fixed displacement parameters to prevent the displacement parameters from expanding to unreasonable sizes. As the structure neared convergence, individual anisotropic displacement parameters of problematic atoms were released if they stabilized at reasonable values, producing some atoms with a mix of variable and fixed parameters. Anisotropic displacement parameters which could not be released were arbitrarily fixed at 0.09. The use of larger displacement parameters produced refinements with a better R value ($R = 0.037$ was achieved by allowing some equivalent anisotropic displacement parameters to expand as large as 15 Å²), but a refinement with smaller displacement parameters was considered more reasonable. The tendency toward large displacement parameters is representative of the disordered nature of the interlayer region. The position of many of the sites identified in the interlayer region are in close agreement with those of Eggleton and Guggenheim (1986); however, several additional positions have been added to the new crystal structure. Due to the problematic nature of positions in the interlayer region, a damping factor of 0.5 was added to the refinement to

---

[1]For a copy of Table 3, Document AM-99-018, contact the Business Office of the Mineralogical Society of America (see inside front cover of recent issue) for price information. Deposit items may also be available on the American Mineralogist web site (http//www.minsocam.org or current web address).

TABLE 2. Atomic positions, isotropic displacement parameters, and occupancies

	x/a	y/b	z/c	Uiso*	Occ.
K1	0.258(1)	0.3524(5)	0.0585(2)	0.065(2)	0.205(5)
K2	0.956(2)	0.385(1)	0.0309(6)	0.096(4)	0.151(6)
K3	0.361(3)	0.348(1)	0.0480(5)	0.079(2)	0.104(4)
Mn1A	0.99203(9)	0.06124(4)	0.23549(2)	0.0095(2)	0.741(2)
Mn1B	0.9984(2)	0.0645(1)	0.24181(5)	0.0066(4)	0.256(2)
Mn2A	0.4982(1)	0.18810(4)	0.24734(2)	0.0094(2)	0.708(2)
Mn2B	0.4921(2)	0.1844(1)	0.23755(5)	0.0095(4)	0.283(2)
Si1	0.8002(1)	0.44606(6)	0.15160(3)	0.0112(2)	0.946(4)
Si2A	0.8159(2)	0.21867(8)	0.13916(4)	0.0143(3)	0.713(4)
Si2B	0.7534(4)	0.2176(2)	0.13407(9)	0.0044(7)	0.255(4)
Si3	0.2976(2)	0.10531(8)	0.12889(4)	0.0119(3)	0.634(4)
Si4	0.4870(4)	0.9319(2)	0.06368(8)	0.0083(6)	0.330(4)
Si5	0.5570(4)	0.0718(2)	0.06243(9)	0.0098(7)	0.306(5)
O1A	0.599(1)	0.1775(4)	0.1015(2)	0.021(2)	0.376(9)
O1B	0.5138(7)	0.1768(3)	0.1167(1)	0.021(1)	0.546(9)
O2A	0.0552(7)	0.1710(3)	0.1147(1)	0.027(1)	0.625(9)
O2B	0.956(1)	0.1672(5)	0.0993(2)	0.018(2)	0.336(9)
O3	0.8127(5)	0.3347(2)	0.12518(9)	0.0253(7)	0.968(9)
O4	0.0339(4)	0.5068(2)	0.12930(9)	0.0257(7)	0.979(9)
O5A	0.7646(8)	0.9689(4)	0.0704(2)	0.014(1)	0.379(8)
O5B	0.7923(6)	0.9853(3)	0.0880(1)	0.015(1)	0.552(9)
O6	0.3153(3)	0.0676(2)	0.19249(8)	0.0226(6)	1.106(9)
O7	0.8199(3)	0.1965(1)	0.20062(8)	0.0181(6)	1.036(8)
O8	0.8239(3)	0.4409(1)	0.21748(7)	0.0128(5)	1.007(9)
O9	0.3262(3)	0.3207(1)	0.21246(8)	0.0184(6)	1.086(9)
O10A	0.621(1)	0.4100(5)	0.4967(2)	0.028(2)	0.40(1)
O10B	0.75	0.345(1)	0.5	0.069(5)	0.40(2)
O11	0.5	0.5	0.5	0.058(2)	0.51(2)
O12	0.25	0.186(1)	0.0	0.090(4)	0.048(2)
O13	0.75	0.326(2)	0.0	0.0900	0.35(1)

Note: Number in parentheses represents one esd of least significant digit. Anisotropic thermal parameters have been deposited with MSA.
*Equivalent isotropic thermal parameter (Å^2).

TABLE 4. Selected bond distances (Å) and angles

Mn1A-O6	2.159(2)	Mn2A-O6	2.324(2)
Mn1A-O6	2.242(2)	Mn2A-O7	2.206(2)
Mn1A-O7	2.219(2)	Mn2A-O7	2.234(2)
Mn1A-O8	2.181(2)	Mn2A-O8	2.166(2)
Mn1A-O8	2.220(2)	Mn2A-O9	2.128(2)
Mn1A-O9	2.259(2)	Mn2A-O9	2.189(2)
Mn1B-O6	2.221(2)	Mn2B-O6	2.144(2)
Mn1B-O6	2.365(2)	Mn2B-O7	2.105(3)
Mn1B-O7	2.260(2)	Mn2B-O7	2.425(2)
Mn1B-O8	2.122(2)	Mn2B-O8	2.246(2)
Mn1B-O8	2.164(2)	Mn2B-O9	2.139(2)
Mn1B-O9	2.128(2)	Mn2B-O9	2.238(2)

Note: Number in parentheses represents one esd of least significant digit.

gram using crystallographic data from the new subcell refinement. Supercells were created by applying symmetry operators to the subcell positions and adjusting the occupancies of inverted and Si3 tetrahedra according to the desired model. Large supercell refinements in MacTempas were performed by combining several different smaller supercells using the CrystalKit computer program. Because CrystalKit uses orthogonal projections to determine new unit-cells, the β value of 93.93° was changed to 90° in the large supercell simulations. This change in unit-cell constants did not produce a discernible effect in diffracted intensities. Instrument variables were chosen to be consistent with an EM420ST TEM.

EXPERIMENTAL RESULTS

Subcell refinement

The subcell structure was refined to $R = 4.1\%$ using the single-crystal X-ray intensity data. In general, there was good agreement between this refinement and the model proposed by Eggleton and Guggenheim (1986). New positions identified in this refinement include the split positions associated with the Mn1, Mn2, and O10 sites and newly identified sites O11, O12, O13, K2, and K3. The Mn split positions sum to approximately 1, indicating that Mn sites are fully occupied. The O10 site was split into the O10A and O10B positions. They are separated by 1.05 Å, suggesting that they may be too far apart to be considered a split position, but are too close to be simultaneously occupied.

The O11 site is located in the inverted region, in the position that Kato (1980) identified as the interlayer cation site. This site was modeled as an oxygen position and refined to an occupancy of 0.7; however, this position may actually be filled by a water molecule. The quality of the refinement was not sufficient to identify the presence of H atoms. However, the presence of H would increase the scattering factor of this position and result in an occupancy for water molecules of approximately 2/3. This corresponds neatly with the occupancy of 1/3 identified for the inverted tetrahedral positions. The sites O12 and O13 also lie in the interlayer, but they are outside of the inverted region. These positions were modeled with oxygen scattering factors, but the types of atoms occupying these sites could not be reliably determined from the electron density. Because they are not associated with a coordination polyhedron, these positions may be filled by water molecules.

Interlayer cation sites were modeled with K scattering factors, as in the refinement of Eggleton and Guggenheim (1986).

aid convergence of the structure. Selected bond lengths and angles are presented in Table 4. Due to the split occupancies and difficulties of refining some of the Si positions, bond lengths and angles were not always reasonable for Si sites. Calculated bond lengths ranged from 1.266 to 2.094 Å, reflecting the averaged values of the reported positions. These values are associated with tetrahedra that have split positions and with the inverted tetrahedra, and they are thought to reflect the disordered nature of the structure. Si bond length and angles are therefore not presented in Table 4.

HRTEM and SAED

HRTEM and SAED were performed with a Philips EM420ST TEM located in the Johns Hopkins University Department of Earth and Planetary Sciences and operated at 120 keV. Powder mounts were prepared by crushing single crystals of ganophyllite in an agate mortar. The resulting powder was mixed in ethyl alcohol, and holey carbon grids were dipped into the suspension. Analytical data were collected using an energy dispersive spectroscopy (EDS) system with an Oxford Analytical detector and Princeton Gamma-Tech System IV spectrum analyzer. The data were reduced as described by Livi and Veblen (1987). Analytical errors are difficult to quantify, but are believed to be within approximately 5% of the analyzed concentrations for the major constituents.

Image and SAED simulations

Image and SAED simulations were performed with the EMS set of programs (Stadelmann 1987) and the MacTempas pro-

TABLE 5. Selected AEM analyses

	1	2	3	4	5
Si	36.22	36.80	36.44	39.32	38.98
Al	9.21	9.13	9.64	10.65	9.94
Na	2.38	1.41	1.63	1.68	2.67
K	0.28	1.90	0.28	0.57	0.22
Ca	0.75	1.00	0.98	0.82	0.95
Mn	24.00	24.00	24.00	24.00	24.00
Mg	0.00	0.00	0.00	0.00	0.00
Fe	0.19	0.24	0.42	0.42	0.64

Notes: Analyses correspond with locations in Figure 11. Data normalized to 24 Mn atoms per formula unit. See text for a discussion of errors.

Subsequently, AEM data (Table 5) indicated that samples from this aliquot of material contain considerably more Ca than K, with lesser amounts of Na. Fourier difference maps indicated the presence of various diffuse areas of electron density in the interlayer region that are consistent with additional, low-occupancy interlayer cation sites. Additional K sites (K2 and K3) were added to areas that supported occupancies of 0.1 or greater. It would be possible to add more such sites with lower occupancies, but they would not add significantly to the refinement.

Although the previous refinement of ganophyllite (Eggleton and Guggenheim 1986) found the Si3 site to be split into two positions, splitting was not indicated here. Eggleton and Guggenheim (1986) also found two non-equivalent sites at the apices of the inverted tetrahedra; only one position was identified here.

AEM data were normalized to 24 Mn atoms per unit-cell (Table 4). These data indicate that there is an excess of Si and Al over what is required to fill the tetrahedral positions, suggesting that some of the Al may enter the octahedral sites; this may result in the splitting of the Mn sites. The Mn1B and Mn2B positions are offset from the center of the octahedra relative to the higher-occupancy Mn1A and Mn2A positions. Because Al would be underbonded in the stable Mn1A position, the Mn1B position may reflect the need for increased bonding of Al atoms in the octahedral sites.

The occupancies of the Si2 positions are in good agreement with the split in Mn positions, suggesting that these phenomena are related. The split in the O5 position is related to the occurrence of inverted tetrahedra. Two thirds of the O5 sites are shared between an Si3 tetrahedron and an inverted tetrahedron in a neighboring [100] strip; one third of the O5 sites are shared by adjacent inverted tetrahedra without an Si3 tetrahedron. Similarly, the split in the O1 and O2 positions should be related to the periodic inversions and absence of the Si3 site.

A few of the silicate bond lengths and O-Si-O angles are not optimal. These values are associated with tetrahedra that have split positions and with the inverted tetrahedra, and they are thought to reflect the disordered nature of the structure.

Supercell modeling

Because the intensity of supercell reflections was too weak for collection by the CAD4, the supercell was modeled based upon the SAED patterns. SAED patterns have an advantage over X-ray diffraction in that electrons are more strongly scattered than X-rays, producing diffraction patterns in which the supercell spots have much greater intensity. The stronger interaction produces dynamic rather than kinematical diffraction conditions, however, and reduces the amount of symmetry in-
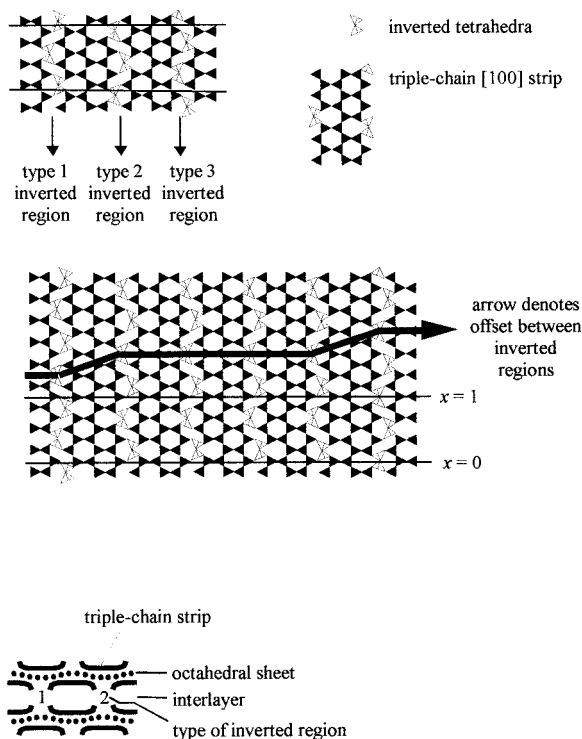

FIGURE 3. Key to successive figures. (**a**) [001] view of tetrahedral strips. (**b**) [100] view of structure.

formation that can be determined from the pattern.

Several different structural models were tested with different arrangements of inversions in the [100] strips. As mentioned previously, these strips are three tetrahedral chains wide with inversions occurring along the outside fringe. The outside fringe of any given strip is located adjacent to the outside fringe from a neighboring strip; inverted tetrahedra in adjoining fringes do not occur immediately across from one another but are offset by $a/2$ (Fig. 3). Inverted tetrahedra along the fringes also share apical O atoms with inverted tetrahedra from fringes across the interlayer gap. Inverted regions are therefore created from the outside fringes of four different [100] strips. The location of inverted tetrahedra is fixed within any given inverted region by the selection of inverted tetrahedra in any of its component fringes (in the case of the adjoining fringe by the required $a/2$ offset and in the case of fringes across the interlayer gap by the need to share apical O atoms).

Inverted regions extend along [100] and are separated by the [100] strips. Although the pattern of tetrahedral inversions is fixed within any given inverted region, inverted regions at either edge of a [100] strip can be shifted by 0 or $\pm a/3$ (the $a/3$ shift arises from the threefold modulation along **a**). The combination of $a/3$ shifts (offset strips) with 0 shifts (non-offset strips) produces a large variety of possible polytypes. Additional polytypes can be created by doubling the **c** axis, as is the case with commensurate ganophyllite. It should be noted that the ganophyllite subcell consists of two layers along [001], so doubling **c** actually produces four layers in the unit cell.
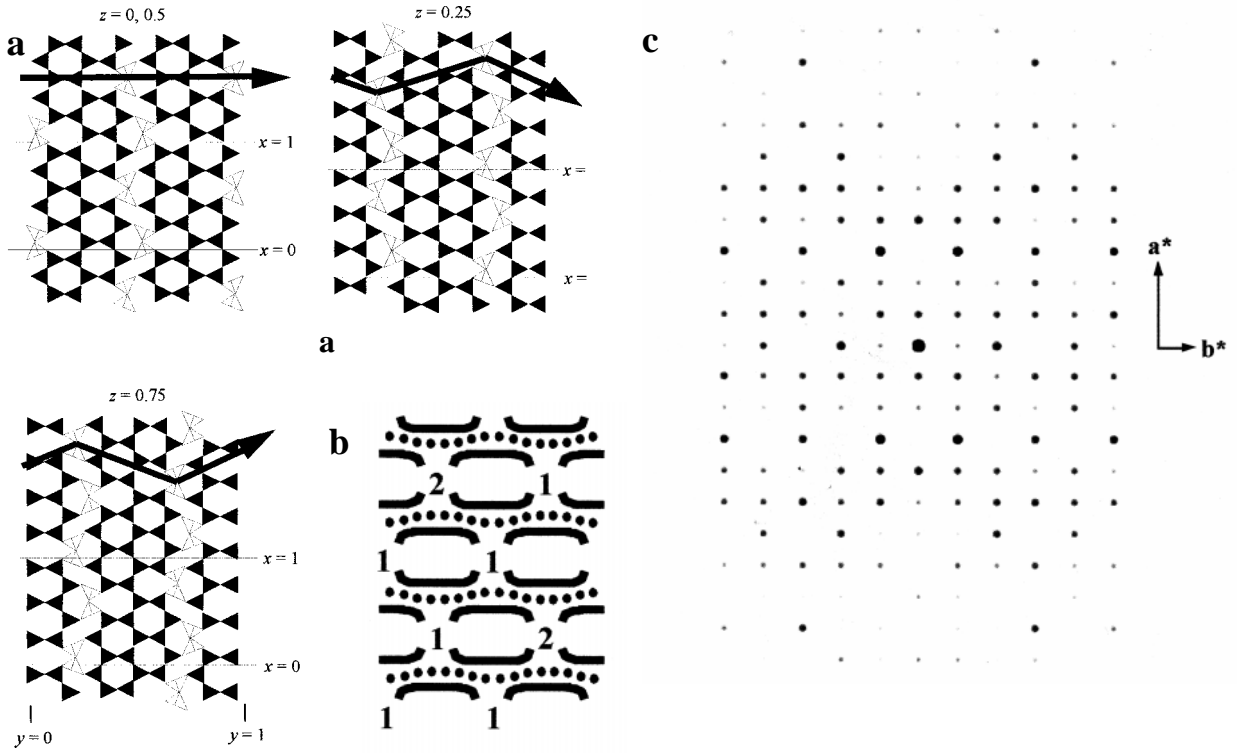
FIGURE 4. Four-layer commensurate cell (type1). **(a)** [100] view of tetrahedral strips (not to scale). **(b)** [100] view of cell (not to scale). **(c)** Simulated [$hk0$] diffraction pattern of this structure.
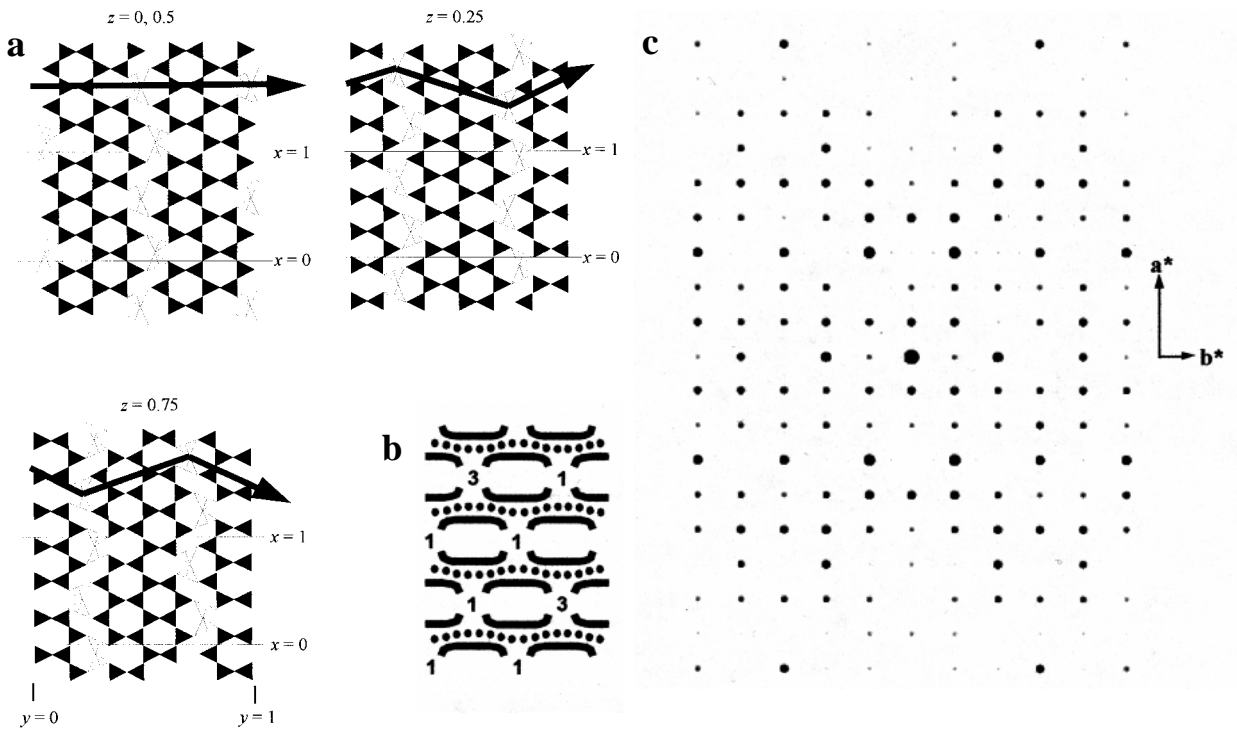

FIGURE 5. Four-layer commensurate cell (type 2). **(a)** [100] view of tetrahedral strips (not to scale). **(b)** [100] view of cell (not to scale). **(c)** Simulated [$hk0$] diffraction pattern of this structure.

Models based upon the proposed monoclinic supercell of Eggleton and Guggenheim (1986) produced simulated SAED patterns that agreed well with the experimentally derived commensurate patterns (Figs. 4 and 5). These models (1920 atoms) had supercells that were tripled along the subcell **a** axis, doubled along the subcell **b** axis, and doubled along the subcell **c** axis (producing four layers along [001]). There are three different models consistent with the monoclinic supercell, two of which are almost identical. All models have four layers along [001] and are two [100] strips wide. All three models have similar layers at $z = 0$ and $z = 0.5$, consisting exclusively of non-offset [100] strips, and all have offset strips in layers at $z = 0.25$ and $z = 0.75$. The primary difference between the models concerns the location along x of inverted tetrahedra in layers with offset strips relative to layers with non-offset strips. In type 1 structures (two of which are possible), inverted tetrahedra in layers at $z = 0.25$, 0.75 occur at approximately the same position along a as those in layers at $z = 0$, 0.5 in one of the [100] strips, but not in the other [100] strip. In type 2 structures (only one of which is possible), inverted tetrahedra in layers at $z = 0.25$, 0.75 never occur in the same position along x as those in layers at $z = 0$, 0.5. Because the simulated diffraction patterns from both models were identical, this aspect of polytypism was not considered in subsequent models.

Models based upon the proposed triclinic supercell of Eggleton and Guggenheim (1986) produced simulated diffraction patterns that were not in good agreement with experimen-

tally derived patterns. Supercell reflections in the simulated patterns demonstrated an angle of "incommensurate" rotation greatly exceeding that found in natural samples and the elimination of A centering produced extra diffraction spots in rows with $h = 3n$. Extra, weak diffraction spots in some of the $h \neq 3n$ rows related to the tripling of the (subcell) **b** axis were also present. The supercell for this model was not doubled along [001], producing a cell that had two layers along [001] instead of four. In both layers, adjacent [100] strips were offset by **a**/3, due to the arrangement of inverted tetrahedra.

To reduce the angle of incommensurate rotation, non-offset strips were introduced between the offset strips. Models were created with one non-offset strip added adjacent to each offset strip in both levels along [001], producing cells that were six [100] strips wide. Simulated SAED patterns from these models had a smaller degree of "incommensurate" rotation, but they still exceeded that found in the experimental SAED patterns. In addition, the sixfold modulation along **b** increased the number of supercell diffraction spots, producing extra spots in rows of $h \neq 3n$. Additional non-offset strips were added, to a maximum of twelve strips used in this study. This model (5760 atoms) produced a simulated pattern that contained the correct geometry for subcell reflections, but supercell reflections were not consistent with experimentally derived patterns (Fig. 6). These reflections appeared to exhibit some degree of incommensurate rotation, but intense supercell reflections (in rows of $h = 3n \pm 1$) were found *between* subcell reflections (in rows
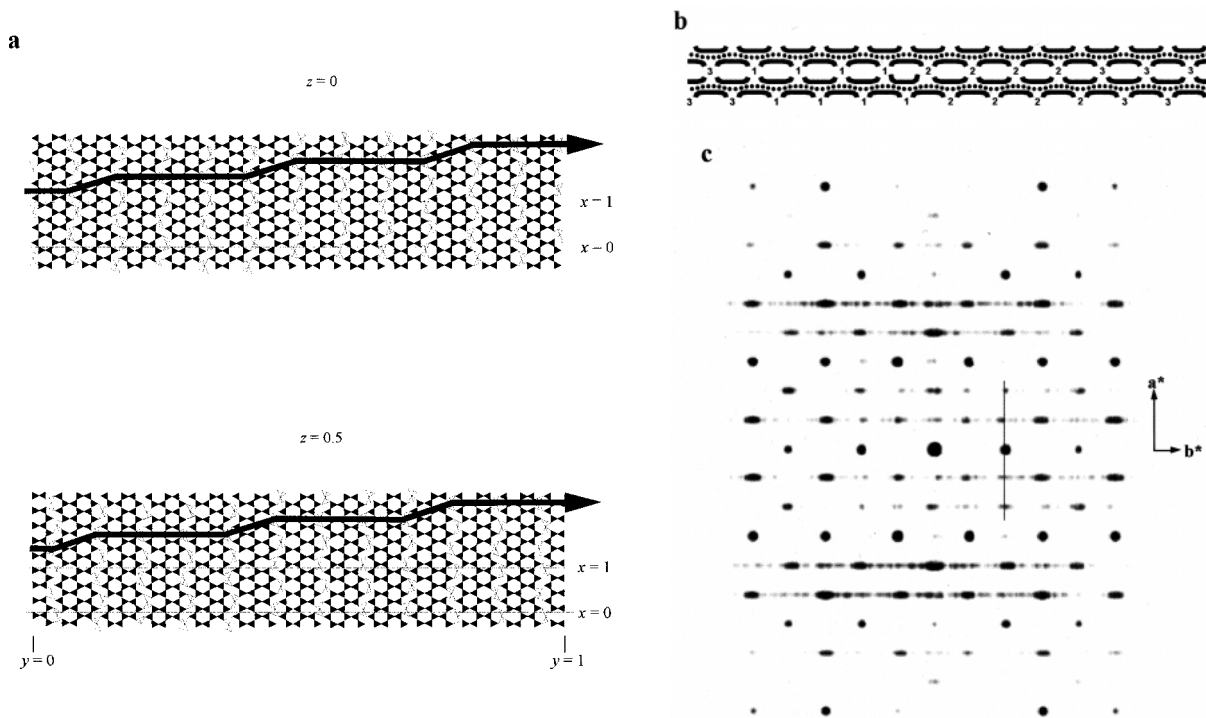

FIGURE 6. Two-layer "incommensurate" cell with a periodic offset in both layers. **(a)** [001] view of tetrahedral strips (not to scale). **(b)** [100] view of cell (not to scale). **(c)** Simulated [$hk0$] diffraction pattern of this structure.

real [hk0] SAED pattern

a*

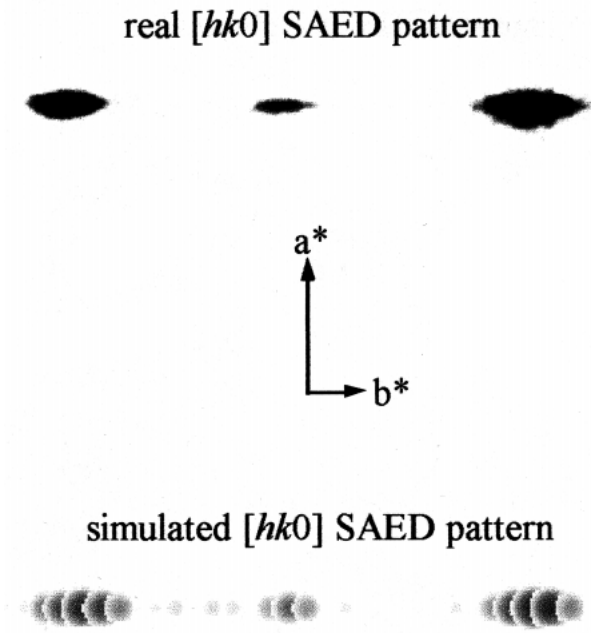**b***

simulated [hk0] SAED pattern

FIGURE 7. Clusters of spots in incommensurate crystals. Supercell reflections from real and simulated [hk0] diffraction patterns are shown. Note the overlapping spots visible in the simulated pattern. Supercell reflections in incommensurate crystals are actually clusters of relatively intense spots.

of $h = 3n$). Intense supercell reflections in experimental patterns are found almost *adjacent* to subcell reflections (Fig. 2B). Supercell reflections did exhibit streaking along b^*, however, which is found in experimental patterns. A careful examination of these reflections resolved the problem associated with extra supercell diffraction spots from earlier simulations with fewer [100] strips. The 12-fold modulation along b produced supercell reflections that were extremely closely spaced. In fact, the SAED simulations indicate that supercell reflections experimentally observed in "incommensurate" samples actually consist of clusters of strong adjacent reflections (Fig. 7).

To resolve the discrepancy with supercell reflections, a new model was tested. This model was based upon a cell which has two layers along [001]; one of the layers was offset as in the previous model, but the other layer contained exclusively non-offset strips (Fig. 8). This model (5760 atoms) produced an arrangement of intense supercell reflections that was in good agreement with experimentally observed patterns. There was only one apparent discrepancy between simulated and experimental patterns, involving weak subcell reflections. In $hk0$ SAED patterns, intense subcell reflections occur at $k = 4n$ for rows of $h = 6n$, and at $k = 4n + 2$ (notation relative to a commensurate supercell that is tripled along the subcell a and doubled along the subcell b) for rows of $h = 6n + 3$. Weak subcell reflections are commonly observed halfway between the intense subcell reflections along b^*; in particular reflections at 020 are 0,10,0 are commonly observed. These reflections were interpreted by Eggleton and Guggenheim (1986) as arising from multiple diffraction. In the simulated SAED patterns of "incommensurate"
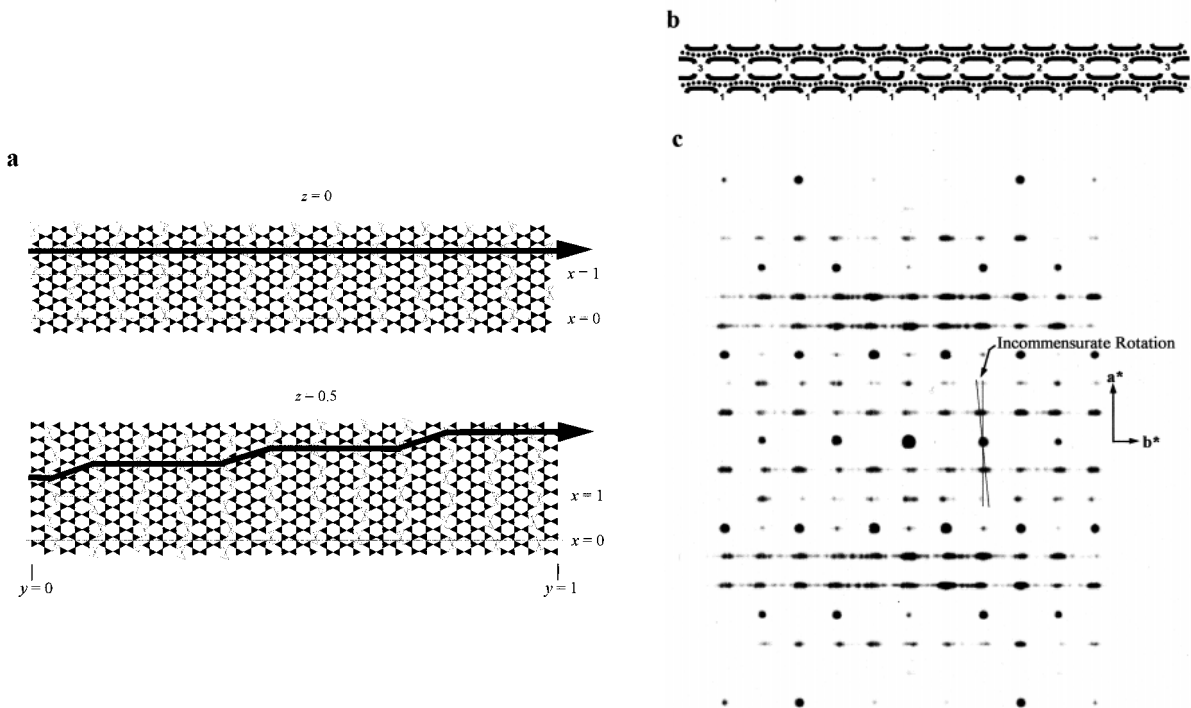
a

$z = 0$

$x = 1$
$x = 0$

$z = 0.5$

$x = 1$
$x = 0$

$y = 0$ $y = 1$

b

c

Incommensurate Rotation

a*

b*

FIGURE 8. Two-layer "incommensurate" cell with a periodic offset in one layer. **(a)** [001] view of tetrahedral strips (not to scale). **(b)** [100] view of cell (not to scale). **(c)** Simulated [hk0] diffraction pattern of this structure.
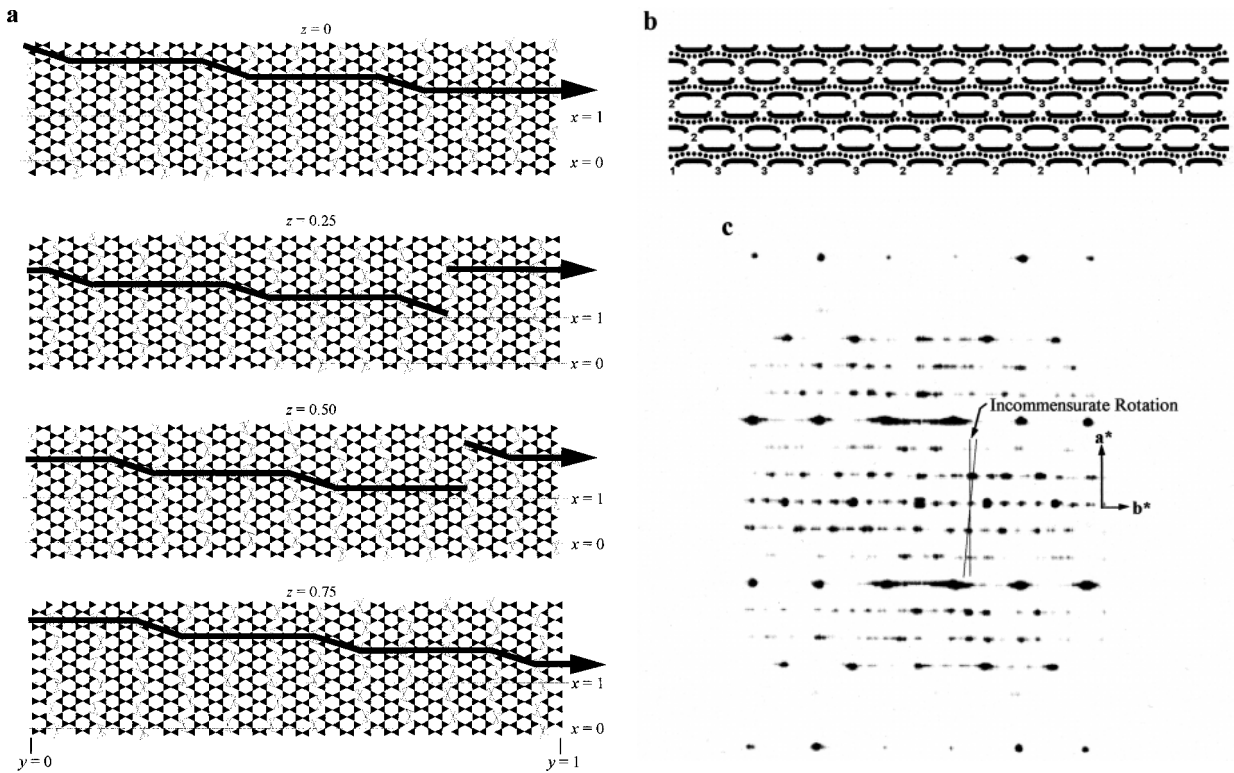
FIGURE 9. Four-layer "incommensurate" cell with periodic offsets in all four layers and A centering. **(a)** [001] view of tetrahedral strips (not to scale). **(b)** [100] view of cell (not to scale). **(c)** Simulated [hk0] diffraction pattern of this structure.
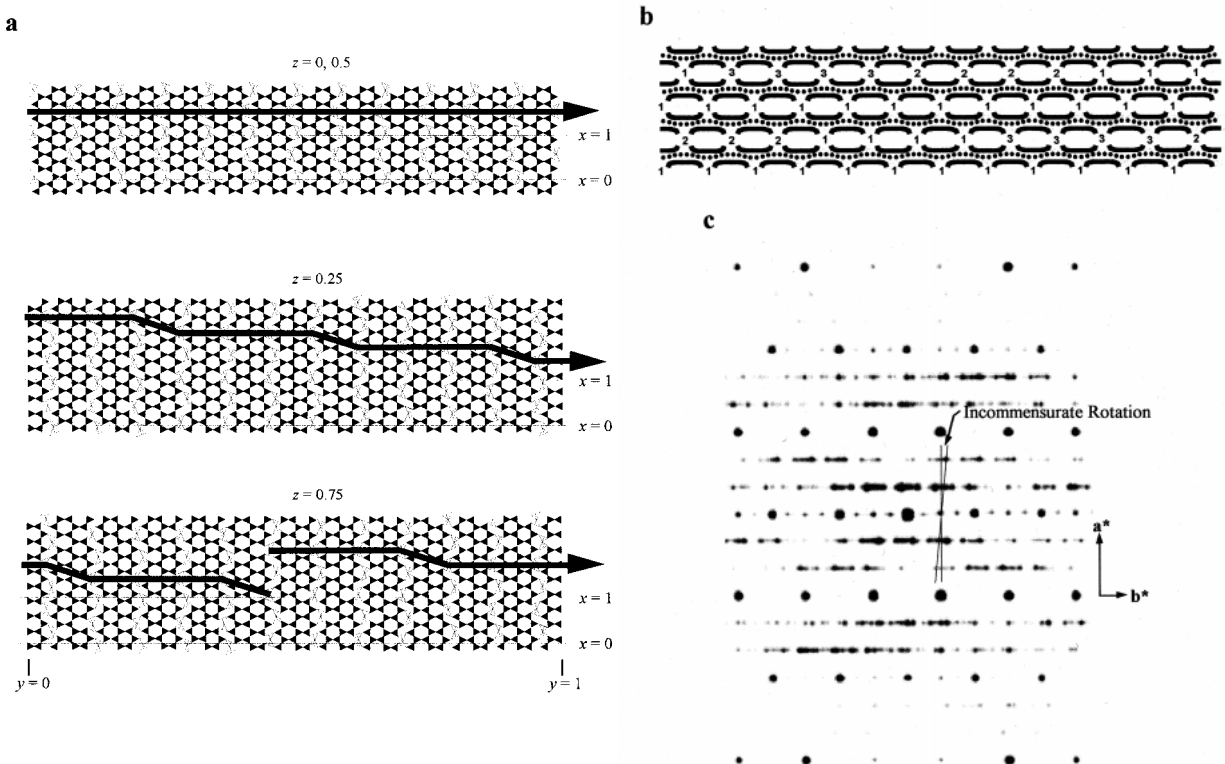

FIGURE 10. Four-layer "incommensurate" cell with periodic offsets in two layers and A centering. **(a)** [001] view of tetrahedral strips (not to scale). **(b)** [100] view of cell (not to scale). **(c)** Simulated [hk0] diffraction pattern of this structure.

ganophyllite, these reflections were not present.

The weak 020 and 0,10,0 reflections are present in the simulated SAED patterns of commensurate ganophyllite. The commensurate models had an *A*-centered supercell, which is not possible in two-layered structures with periodic offsets. Although the triclinic form described by Jefferson (1978) had a supercell that was not doubled along [001] (and therefore had two layers along [001]), models were tested that were doubled along [001] to produce four-layered structures that could have *A*-centering. Models in which all four layers were periodically offset (11 517 atoms) (Fig. 9) produced supercell reflections that had the wrong pattern of intensities, as for the corresponding two-layer model. Models in which two of the layers were periodically offset (11 517 atoms) (Fig. 10) produced supercell intensities that were more correct than the previous model, but the clusters of intense reflections were wider along **b*** than for the corresponding two-layer model and provided a poorer match with experimental SAED patterns. In addition, weak supercell reflections were produced for all $k = n$ along the $h = 0$ and $h = 6$ rows of reflections, which is not consistent with natural SAED patterns. Both of the *A*-centered models with four layers along [001] were 12 [100] strips wide.

Although the appearance of weak 020 and 0,10,0 reflections (relative to the commensurate supercell) could not be resolved by these models, HRTEM combined with SAED provides clues to their origin. Samples for this investigation were prepared by crushing millimeter-scale crystals. The resulting powder contained both commensurate and "incommensurate" crystals that were micrometer-scale in length, based upon TEM and SAED analysis of the powder. Some micrometer-scale crystals could be seen to contain both commensurate and "incommensurate" regions, based upon the smallest SAED resolution possible with the 420ST TEM (~25 μm; Fig. 11). Many crystals probably contain nanometer-scale intergrowths that are too small to resolve with convention SAED methods. Natural samples that appear "incommensurate" but display weak 020 and 0,10,0 reflections probably have small commensurate regions.

AEM results

AEM data indicate significant variations in composition not just between crystals but within single crystals (Table 5). These data suggest that the presence of "incommensurate" modulation is not related to the type or amount of interlayer cation present, Al/Si ratios, tetrahedral cation/Mn ratios, or any other identified compositional variables.

HRTEM images

HRTEM images clearly demonstrate the threefold modulation along **a** as light and dark fringes that extend in lines parallel
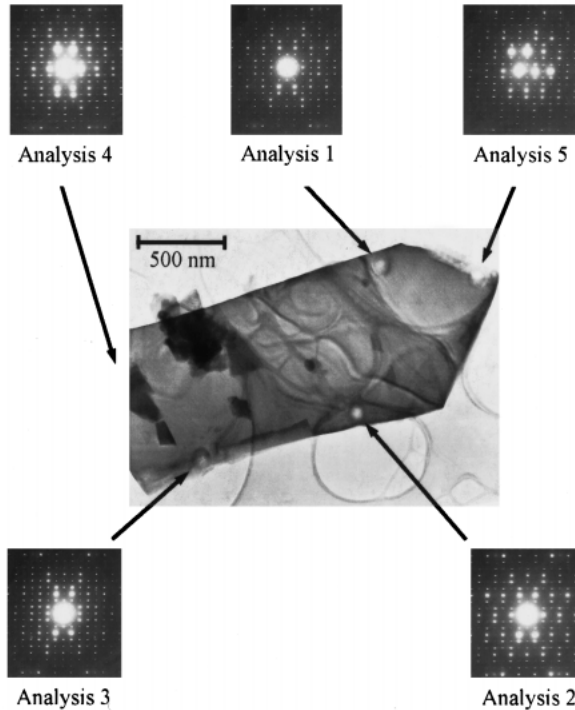

FIGURE 11. [*hk*0] SAED patterns showing commensurate and incommensurate regions in a "single" crystal. Rotation of diffraction patterns does not necessarily match that of crystal. Chemical data for these areas is presented in Table 4.
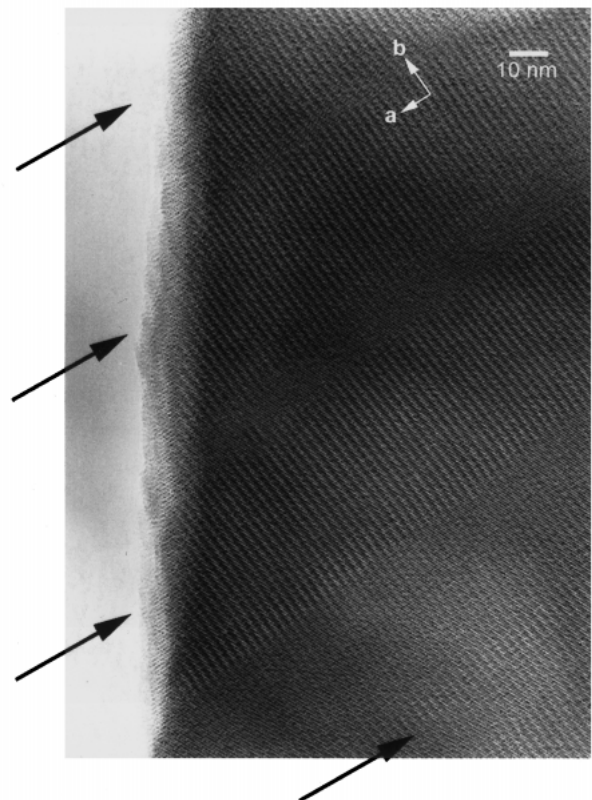

FIGURE 12. Bands of modulation that extend parallel to **a** (marked by arrows).

to **b**. Images from numerous crystals have shown that these fringes are not continuous in incommensurate crystals, but are broken up into bands that extend parallel to [100] (Fig. 12). These bands vary from approximately 150 to 500 Å in width, with individual fringes commonly becoming slightly curved near the margins. Commensurate crystals are also sometimes found to display this band-like morphology, but more commonly display continuous fringes. "incommensurate" crystals have not been observed with continuous fringes. The band-like morphology may be related to the presence of offset strips. The simulated models contained offset strips that were separated by up to three non-offset strips. In real ganophyllite, multiple offset strips might occur in adjacent positions, producing entire areas that are offset. Although the ratio of non-offset to offset strips has been shown to be at least 3 to 1, the arrangement of these strips along [010] may be essentially random. The simulated models that best matched experimental SAED patterns contained twelve [100] strips, producing a **b** axis that is 162.5 Å in length, which places them in the lower bound of observed domain sizes.

REFERENCES CITED

Eggleton, R.A. and Guggenheim, S. (1986) A re-examination of the structure of ganophyllite. Mineralogical Magazine, V50, p.307–315.
——(1994a) Structure and polytypism in bementite; a modulated layer silicate. American Mineralogist, 79, 91–106.
——(1994b) The use of electron optical methods to determine the crystal structure of a modulated phyllosilicate: parsettensite: American Mineralogist, 79, 426–437.
Ferrow, E.A. and Hovmøller, S. (1993) Crystallographic image processing (CIP) and High Resolution Transmission Electron Microscopy (HRTEM) studies of bannisterite, a modulated 2:1 layer silicate. European Journal of Mineralogy, 5, 181–188.
Guggenheim, S. and Eggleton, R.A. (1994) A comparison of the structures and geometric stabilities of stilpnomelane and parsettensite: A distance least-squares (DLS) study. American Mineralogist, 79, 438–442.
Hall, S.R., Flack, H.D., and Stewart, J.M., Eds. (1992) Xtal3.2 Reference Manual. Universities of Western Australia, Geneva, and Maryland.
Hamberg, A. (1890) Uber ganophyllite, ein manganzeolith von Harstigen. Geologiska Föreningens i Stockholm Förhandlingar, 12, 586–598.
Heaney, P.J., Post, J.E., and Evans, H.T. Jr. (1992) The crystal structure of bannisterite: Clays and Clay Minerals, 40, 129–144.
Jefferson, D.A. (1978) The crystal structure of ganophyllite, a complex manganese aluminosilicate. I. Polytypism and structural variation. Acta Crystallographica, 34, 491–497.
Kato, T. (1980) The crystal structure of ganophyllite, monclinic subcell. Mineralogical Journal, 10, 1–13.
Livi, K.J.T. and Veblen, D.R. (1987) "Eastonite" from Easton, Pennsylvania: A mixture of phlogopite and a new form of serpentine. American Mineralogist, 72, 113–125.
Merlino, S., Ed. (1997) EMU Notes in Mineralogy, Vol. 1. Eøtvøs University Press, Budapest, Hungary.
Peacor, D.R., Dunn, P.J., and Simmons, W.B. (1984) Eggletonite, the Na analogue of ganophyllite. Mineralogical Magazine, 48, 93–96.
Post, J.E. and Veblen, D.R. (1990) Crystal structure determinations of synthetic sodium, magnesium, and potassium birnessite using TEM and the Rietveld method. American Mineralogist, 75, 477–489.
Smith, M.L. and Frondel, C. (1968) The related layered minerals ganophyllite, bannisterite, and stilpnomelane. Mineralogical Magazine, 36, 893–913.
Stadelmann, P. (1987) EMS—a software package for electron diffraction analysis and HREM image simulation in materials science. Ultramicroscopy, 21(2), 131–145.